ORIGINAL RESEARCH PAPER

Chemistry

Volume : 6 | Issue : 11 | November 2016 | ISSN - 2249-555X | IF : 3.919 | IC Value : 74.50

Biodegradable Polymer Nanocomposites Based on polyvinyl alcohol and Nano-Rice Straw

KEYWORDS

Polyvinyl alcohol; Nano-rice straw; Biodegradable; UV-degradation; nanocomposite films.

E. M. Abdel Bary

Chemistry Department, Faculty of Science, Mansoura University, Mansoura, Egypt

Yaser A. Soliman

Department of Chemistry, Faculty of Science, Amran University, Yemen

Ahmed Fekri

Chemistry Department, Faculty of Science, Mansoura University, Mansoura, Egypt

Ammar N. Harmal

Department of Chemistry, Faculty of Science, Amran University, Yemen

ABSTRACT The effect of nano-rice straw (NRS) on the mechanical, thermal and biodegradable properties of PVA/NRS nanocomposite films has been investigated. NRS was chemically modified with maleic anhydride (MA). The biodegradability of PVA/NRS nanocomposite films was evaluated under UV accelerated weathering tester as well as soil burial test. Fourier-Transformation Infrared (FTIR) spectroscopy as well as wide-angle x-ray diffraction have been used to characterize the structure of PVA/NRS nanocomposite. Thermal analysis [differential scanning calorimetry (DSC)] was employed to characterize and reveal the thermal behavior and the structural properties of such PVA/NRS nanocomposite. Scanning Electron Microscope (SEM) was used to characterize the morphology of PVA/NRS nanocomposite films. It has been found that the nano- rice straw improved both the mechanical and biodegradability of nanocomposite samples.

1. Introduction

Many research topics are directed towards getting more highly engineered wood polymer composites having high performance, more efficient design and possesses biodegradability. The convention biodegradable polymers include polyvinyl alcohol (PVA), poly caprolactone (PCL), poly(butylene succinate) (PBS), polylactic acid (PLA), polyhydroxyalkanoates (PHA) and others (Tighzert, l. Vroman 2009; Sakurada 1985). PVA is a semicrystalline, hydrophilic polymer, has low toxicity [3], good mechanical properties , and is produced on a large scale (Allison et al. 2015; Leja and Lewandowicz 2010). One of the advantage of PVA is that it is biodegradable in physiological environments [5]. PVA with other biodegradable polymers, such as polysaccharides may result in versatile biodegradable plastics with a wide spectrum of properties. Moreover, PVA can be used either in the industrial packaging field or the biocompatible/bioabsorbable medical device market[6]. It can be easily shaped into molded parts, film or fiber forming and others [1]. Rice straw, which is renewable and biodegradable, is the most abundant natural biopolymer in the world (Purwar et al. 2015; Qiu and Netravali 2012). Rice straw at the nano- and micro-scale have much better mechanical properties and are suitable for the reinforcement of some polymers (Wu et al. 2012; Lawal, Balogun, and Akpan 2012). Some authors used several natural products treated with high-intensity ultrasonication to compound PVA nanocomposites at room temperature and found that the tensile modulus and strength of PVA were increased by the addition of the rice straw [11]. However, the compatibility between PVA and rice straw still needs to be improved by creating interfacial adhesion between PVA matrix and rice straw fibers This study is aiming to improve the interfacial adhesion between rice straw and PVA and evaluate biodegradable properties of PVA reinforced with NRS. Besides, special attention is paid to evaluation of ultraviolet degradation

2. Materials

Polyvinyl alcohol, (PVA, [degree of polymerization: 17,000–18,000; and hydrolyzed between 99.0% and 99.8% from PVAc is obtained from M/s. Loba Chem (India).

Rice straw from Farm of the Faculty of Agriculture, Mansoura University.

Maleic anhydride, LOBA Chemie Pvt. Ltd., Mumbai, India.
Glutaraldehyde (25% content in water, extra pure grade).
Glycerin, Sigma-Aldrich Inc. (St Louis MO, USA).

3. Experimental Section

3.1. Treatment of nano- rice straw [NRS]

3.1.1. Mechanical treatment of nano- rice straw [NRS]

The mechanical treatment of rice straw was accomplished through high shearing and compressing forces generated by the pan-mill. The details of the pan-mill equipment and operation procedure was reported [12]. The discharged rice straw fine fibers was then collected for the next milling cycle. After that, the rice straw fine fibers was suspended in water and subjected to ultrasonic treatment for about 45 min using a sonicator (Biologics 150VT, VA) in aqueous medium.

3.1.2. Chemical modification of rice straw

Rice straw was firstly dried at 70 °C for 24 h in a vacuum oven followed by treatment with aqueous solution of NaOH (10 wt %). The rice straw was immersed in the solution for 2h at ambient temperature and then filtered and washed several times with distilled water till neutrality then dried at 70 °C for 24 h in a vacuum oven. The dried rice straw (10 gm) was immersed in a 0.6 N solution of maleic anhydride in xylene (100 ml) and then heated at reflux (140 °C) for 4 hours. The esterified rice straw was filtered from the xylene solution and intensively washed with distilled water in order to eliminate the unreacted maleic anhydride. Finally, the nano-rice straw was dried at 70 °C in a vacuum oven until constant weight was achieved[13].
The added on maleic anhydride on rice straw was calculated by the difference in weight in rice straw before and after treatment

Volume : 6 | Issue : 11 | November 2016 | ISSN - 2249-555X | IF : 3.919 | IC Value : 74.50

where it was achieved 13% ±0.5.

3.2. Preparation of PVA/NRS nanocomposite films

10 gm of PVA was dissolved in 100 ml distilled water at 80 °C for 1h with continuous stirring. GA solution (2.2 vol %) was added at 80 °C for 2h to PVA solution. Also, glycerin (0.87 vol %) was added as plasticizer at 80°C for 30 min to PVA solution. Finally, different loadings of nano-rice straw were added to PVA solution based on the dry content of PVA. The mixture was stirred strongly in a beaker until complete dispersion of the fibers and then preheated at 70 °C for 2 h [8]. After filtering through a 50-mesh sieve, the mixture was oven-dried at 85 °C for 4 h before being hot-pressed (80 °C and 20 MPa) [8]. Different compositions of PVA/ NRS nanocomposite films containing PVA, crosslinked-PVA and the concentrations of nano-rice straw in composite were, 1%, 3%, 5%, 7% and 10% (% by Weight) and designated as PR1, PR2, PR3, PR4 and Pr5.

3.3. Characterization

3.3.1. Fourier transform infrared spectroscopy (FT-IR)

FT-IR absorption spectra were carried out for PVA/NRS nanocomposite films using the Shimadzu FT-IR Spectrophotometer (4 cm^{-1} resolution and 16 scans), at room temperature. FT-IR spectra of the PVA/NRS nanocomposite films were obtained in the spectral range of 4000-400 cm^{-1}.

3.3.2. X-ray Diffractometry

X-ray diffraction scans were obtained using (XRD) PW 150 (Philips) using Ni filtered Cu K radiation (where, = 1.540 Å, the tube operated at 40 kV,30 mA and the Bragg's angle (2) in the range of 0-60). In this analysis, the peak locations (2) in X-ray diffraction spectra are used to identify the different crystalline structures in the pure and polymeric nanocomposite films.

3.3.3. Transmission electron microscopy

Transmission electron microscope (TEM) image and particle size were obtained using a (JEOL JEM-1230 operated at 120 KV). For TEM image the nano-filler powder was dispersed in water by using ultrasonic dispersion and a drop of the suspension was placed onto the carbon-coated grids.

3.3.4. Scanning Electron Microscopy (SEM)

The morphology of the PVA/NRS nanocomposite films was characterized by scanning electron microscope using (JEOL JSM-6510LV) operating at 20 kV accelerating voltage. Surface of the PVA/NRS nanocomposite films were coated with a thin layer of gold (3.5 nm) by the vacuum evaporation technique to minimize nanocomposite films charging effects due to the electron beam.

3.3.5. Differential Scanning Calorimetry (DSC)

The thermal transition behavior of the prepared thin PVA/NRS nanocomposite films was determined by Differential Scanning Calorimeter model Schimadzu DSC Q100 V9.4 Build 287 from 0°C to 250°C. A heating rate of 10°C/min was used under nitrogen atmosphere and at a flow rate of 30 mL/min.

3.3.6. Mechanical testing

A testing machine (Zwick Roell Model Z100 Tensile Tester) was used to test the mechanical properties of PVA/NRS nanocomposite films according to ASTM D-412 with a length of 20 mm between the top and bottom clamps, a crosshead speed of 10 0mm/min, and a load cell of 30 kN. All tests were carried out at room temperature (25 ± 2 °C).

3.3.7. Swelling behavior

For swelling measurements, the dried PVA/NRS nanocomposite films were weighed before being immersed in water (W_d). The swelling was carried out at pH 7.4, and 25°C. After immersion for different time periods, the PVA/NRS nanocomposite films were periodically removed from the medium, the surface was blotted with filter paper and the weight of the nanocomposite sample at time t (W_t) was determined. The swelling degree (SD) was calculated according to Eq. (1)

Where W_t is the weight of the nanocomposite after swelling in water for time t and W_d is the weight of the dried PVA/NRS nanocomposite films. Three measurements were performed for each nanocomposite mixture[14].

3.3.8. The weathering test

The weathering test was performed by using an QUV Accelerated Weathering Tester for 0, 50, 100 and 200 h[15]. The irradiation was carried out at 315 - 400 nm and the temperature in the chamber was approximately 50 - 53 °C. Weathering of. PVA/NRS nanocomposite films was carried out using UV-irradiation and heat in this study[16]. The percent degradation in the PVA/NRS nanocomposite films was calculated using the following equation (3)[17].

$$\text{weight loss (\%)} = \frac{(Wo - Wd)}{Wo} \times 100 \qquad (3)$$

Where, W_o is the initial weight of the dry nanocomposite and W_d is the weight of the degraded nanocomposite.

3.4. Soil burial test

3.4.1. Preparation of Test Medium

The dry soil was ground to a powder after removal of coarse aggregates, stones, and macro organisms by sifting. The dry soil was then supplemented with urea (6 g/kg) to encourage an active microbial flora. The processed soil was then placed in a plastic sack filled with 300 ml of water and the mixture was allowed to stand for 24 h so that the water could fully penetrate the soil. The plastic sack was kept moist with water and stored in the garden at ambient humidity (36 –92%) and temperature (28 – 38 °C).

3.4.2. Test Method for biodegradation

Samples to be tested for biodegradation were dried at 50°C. Each of the accurately weighed dry nanocomposite films was then buried completely into the wet soil of the test medium and left for 60 days where weight loss was measured every five days. The test medium was maintained at temperature (28 – 38 °C) with daily addition of water to replenish any loss due to evaporation. Sequentially, every five days the test PVA/NRS nanocomposite films were removed and washed with water to remove the soil adhered on the surface of the PVA/NRS nanocomposite films dried at 50°C. The percent degradation in the polymers was then calculated using the following equation (3)[17].

$$\text{weight loss (\%)} = \frac{(Wo - Wd)}{Wo} \times 100 \qquad (3)$$

Where, W_o is the initial weight of the dry nanocomposite and W_d is the weight of the degraded nanocomposite.

4. Results and discussion

4.1. Modification of RS with maleic anhydride.

The reaction of maleic anhydride and rice straw was carried out as mentioned before in experimental section. The changes in the chemical structure was followed up by FTIR and the results are given below.

4.1.1 Spectroscopic characterization of NRS by FTIR

RS and NRS were characterized by FTIR spectroscopy to detect the changes in their chemical structure either due uv radiation effects or due to biodegradation. The vibrational bands for -OH stretching of nano-rice straw appear at 3426 cm^{-1} with high intensity and the broad bands are attributed to intramolecular hydrogen bonding from the maleate conformation and -OH bending at 1058 cm^{-1}, while it was appeared at (3420 cm^{-1}) in the

Volume : 6 | Issue : 11 | November 2016 | ISSN - 2249-555X | IF : 3.919 | IC Value : 74.50

case of RS [13]. The band at 1641 cm^{-1} is assigned to C=O in hemicelluloses or lignin. Also, the new band appeared at 1722 cm^{-1} confirms the esterification reaction of the anhydride group with the OH groups in NRS (Fig. 1).

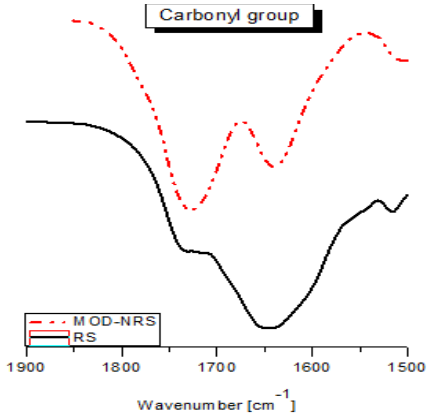

Fig. . FTIR spectra of rice straw [RS] and nano-rice straw [NRS].

4.1.2. Chemical structural characterization by FTIR to PVA, crosslinked- PVA and nanocomposite films

PVA has been crosslinked with GA to get nano composites of crosslinked PVA. This of course improves the water resistant of PVA and improves its mechanical properties. The changes in the chemical structure of PVA as result of its reaction with GA is shown below:

The absence of absorption bands of hydroxyl groups from spectrum of crosslinked-PVA due to the reaction GA with PVA. The increase of the absorbance peak at 1151 cm-1 raised from the formation of an acetal ring and ether linkage as a result of the reaction between the hydroxyl groups [PVA] and the aldehydes [GA].

The absence of a part of -OH group of PVA that formed intermolecular hydrogen bonding which in turn gives rise to polymeric association of OH groups The carboxylic group's bands of NRS are shifted from 1722 cm-1 to 1707 cm-1 due to formation of hydrogen bond in nanocomposite films (table 1).

Table 1. Assignments of the main FTIR signals of non-irradiated PVA, crosslinked- PVA and PVA/NRS nanocomposite films.

regions	PVA		Crosslinked- PVA		Nanorice straw		Nanocomposite (PR2)	
	Values	shape	Values	shape	Values	shape	Values	shape
Hydroxyl groups	-	-	3639	broad, low int.	-	-	3651	Low sharp, low int.
	3589	Low sharp, low int.	3591	v. Low sharp, low int.	-		3591	v. Low sharp, low int.
	3559	v. Low sharp, low int.	3551	v. Low sharp, low	-	-	-	-
	3465	sharp, low int.	-	-	-	-	3460	sharp, high int.
	3429	sharp, low int.	3419	-	3422	broad, low int.	3425	Low sharp, low int.
	3412	v. Low sharp, low int.	-	-	-	-	-	-
	-	-	3365	v. Low sharp, low	-	-	3365	v. Low sharp, low int.
Methylene groups	2942	broad, high int.	2982	v. Low sharp, low int.	2903	high broad, low int.	2969	broad, low int.
	2889	broad, high int.	2850	high broad, high int.	-	-	2843	broad, high int.
Carbonyl groups	1711	v. Low sharp, low int.	-	-	1722	broad, high int.	1707	high broad, high int.
	1657	sharp, high int.	1645	high broad, high int.	1640	sharp, low int.	1601	broad, low int.

4.1.3 Effect of UV irradiation

It is known that UV irradiation should affect the chemical structure of PVA. The change in the chemical structure depends on irradiation dose. FTIR was used to follow up the changes in the chemical structure of PVA subjected to uv radiation. It has been found that a marked loss in the bands at 3589, 3412 and 3342 cm^{-1} in the FTIR spectrum of irradiated neat PVA for 50 and 100 hour indicates the loss of part of -OH groups during irradiation. The absorption bands at 1713 and 1659 cm^{-1} are characteristic to ketones (acetate moiety and/or oxidation during preparation and processing in the non-irradiated PVA spectrum). A general decreasing trend may be observed in the carbonyl region of irradiated PVA, indicating mass loss. The low intensity of bands at 1714 and 1660 cm^{-1} in spectrum of irradiation PVA indicates loss part of C=O structured entities during irradiation and/or due to the low photo stability of the formed ketones which undergo photochemical decomposition [18]. Also, this aspect may be valid for the remaining acetate groups during PVA backbone photocleavage, explained by the lowering in intensity of the carbonyl region (Ferreira, Melo, and Ramos 2010; Wei, Pintus, and Schreiner 2012). Also the impurities and/or oxidation products formed during

Volume : 6 | Issue : 11 | November 2016 | ISSN - 2249-555X | IF : 3.919 | IC Value : 74.50

preparation and processing may represent important initiating sites for photooxidation, From the above, biodegradable PVA partially under the UV irradiation and this is what was observed when studying weight loss[21].

The FTIR spectrum of crosslinked- PVA indicates the formation of intense photooxidation processes during irradiation. The bands containing multiple bands in the range 3601–3327 cm^{-1} corresponds to the formation of new hydroperoxide structures at 3601, 3545, 3464 and 3327 cm^{-1}. The new three bands at 1714,1659 and 1581 cm^{-1} confirm the photo oxidation processes via the formation of new carbonyl structures(acetic and glutaric acids)[22] and is also attributed to the formation of some C=C bonds [23], possibly conjugated with other double bonds or carbonyl and/or carboxyl groups resulted during photodegradation [22]. The weak band of acetal group at 1151 cm^{-1} with low intensity seems to be broken under the effect of UV-irradiation , formed by the cross linking reaction of PVA with GA .

The FTIR spectrum of nanocomposite (PR2) films indicates the occurring of intense photooxidation processes during irradiation. The bands containing multiple bands in the range 3529–3413 cm^{-1} correspond to the formation of new hydroperoxide structures [24] and loss of free hydroxyl groups at 3651 cm^{-1} . The new band in the range 1716–1564 cm^{-1} confirms the occurrence of photo oxidation processes via the formation of new carbonyl structures. [22]. Also, The bands at 1664 cm^{-1} are attributed to the formation of some C=C bonds [23], as mentioned before (Silverstein, Webster, and Kiemle 2005; Varganici et al. 2014) and the band at 1664 cm^{-1} is attributed to C_2— C_3 a-diketones formation which may undergo keto–enol tautomerism. These diketone are responsible for yellowness of nanocomposite and their formation occurs regardless of hydrolysis phenomena in the main nanocomposite backbone [25]. Further photocleavage of the cellulose C_2 — C_3 bonds leads to conjugated unsaturated structures which are further lost during irradiation, this being a specific photoreaction of cellulose under sunlight exposure [25]. In this sense, also the band at 1716 cm^{-1} may correspond to aliphatic aldehyde structures [24]. The results found regarding the photodegradation of the individual cellulosic component are in good agreement with other literature data as photooxidative processes lead to an increase in carboxyl, carbonyl and hydroperoxide groups and a significant lowering of polymerization degree.

4.2. XRD analysis of PVA/NRS nanocomposite films

XRD patterns of PVA/NRS nanocomposite films are shown in (Fig. 2) The XRD curve of PVA film shows only an intense diffraction peak are centered at 2θ = 19.34° degree as a fundamental peak and at 2θ = 40.75° as a secondary peak and which intensities for both fundamental and secondary peaks observed in (Fig .2) and the intensity of the PVA was comparatively higher due to the hydroxyl groups in its side-chains [26]. Intensities of crystallinity of crosslinked-PVA film at 2θ = 19.23° and 40.67° decrease significantly after addition of crosslinking reagent (GA). The peaks for PR1, PR2, PR3, PR4 and PR5 nanocomposite films have only individual widen peak at (PR1, 2θ = 19.27°, 40.39°), (PR2, 2θ = 19.31°, 40.71°), (PR3, 2θ = 19.55°, 40.93°), (PR4, 2θ = 19.57°, 40.39°) and (PR5, 2θ = 18.98 °), as shown in (Figs. 2), respectively. These peak intensity of PVA/NRS nanocomposite films decreases markedly with increase concentration of NRS, and is attributed to the random dispersion of the NRS in the PVA/NRS nanocomposite films, (Ching et al. 2015; Liu et al. 2012;Zhang et al. 2014). No new peaks appeared for NRS ,which indicates the random dispersion of the nano-filler in nanocomposite films[17]

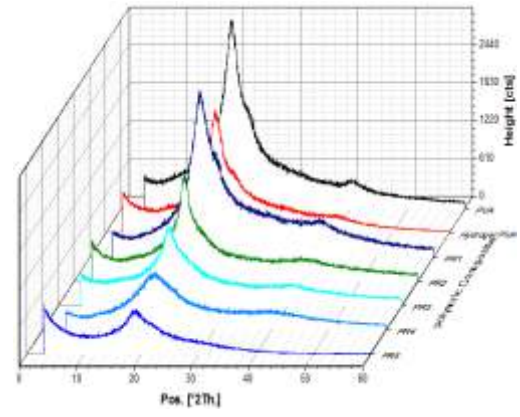

Fig. 2. X-ray diffraction pattern of PVA, crosslinked- PVA and PVA/NRS nanocomposite films.

4.3. Transmission electron microscopy (TEM) of NRS

The chemically modified rice straw enables to have the rice straw in nanoscale. This was confirmed by TEM micrographs shown below (Fig.3). Figure 3 shows TEM micrographs concerning morphology and distribution of the particle size of prepared nano-rice straw. Some particles had sizes in the range 14.75 -64.70 nm. The histogram shows that the nanoparticles exhibited nearly uniform spherical shape and the particle size distribution has the average size of 14.75 -64.70 nm

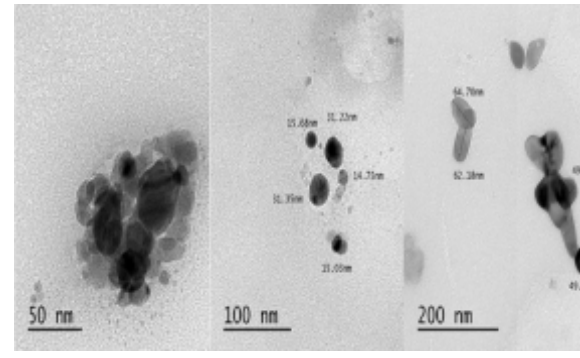

Fig. 3. Transmission electron microscopy for nano-rice straw.

4.4. SEM study of PVA/NRS nanocomposite films

The microstructure of crosslinked- PVA film was studied to investigate the effect of NRS content using scanning electron microscope (SEM). (Fig. 4) shows the SEM micrograph of the surface of crosslinked- PVA, PR1, PR3 and PR5 nanocomposite. For the crosslinked- PVA film, it is clear that it has a uniform surface morphology revealing a rather smooth texture. The nanocomposite films are also uniform, but there are some semi-tori appeared as bright spots in all of them with different degree of roughness and are gradient to disembark in permeability and transparency. These observed uniform distributed bright spots on the secondary electron images shown in the figure shown that the dispersion of the NRS within the polymeric matrix is fairly good with simple aggregate parts of NRS particles, which increase with increasing the concentration of NRS. Also, this indicates segregation of the NRS in the host matrix which may confirmed the interaction and complexation between the NRS and the polymer (Fig. 4). The PR3 nanocomposite film presented visible indication of infestation, corrosion and damaged until 60 days of testing compared with crosslinked-PVA. Attack of the different types of bacterial and fungal colonizate are responsible for corrosion and deterioration of the polymeric blend as reported in the literature[29] (Fig. 4).

Volume : 6 | Issue : 11 | November 2016 | ISSN - 2249-555X | IF : 3.919 | IC Value : 74.50

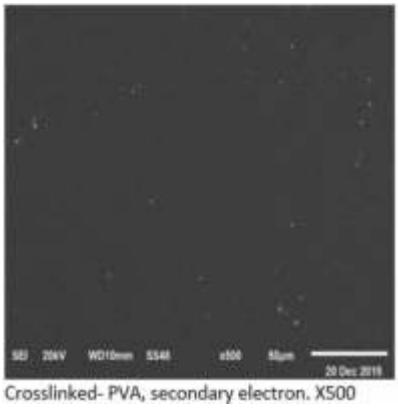

Crosslinked- PVA, secondary electron. X500

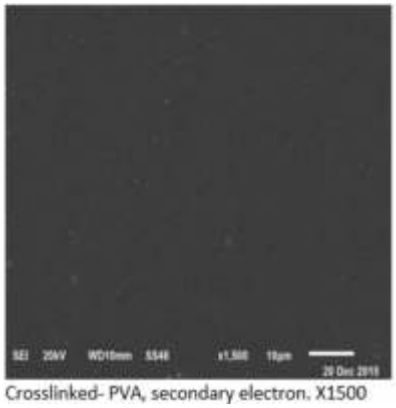

Crosslinked- PVA, secondary electron. X1500

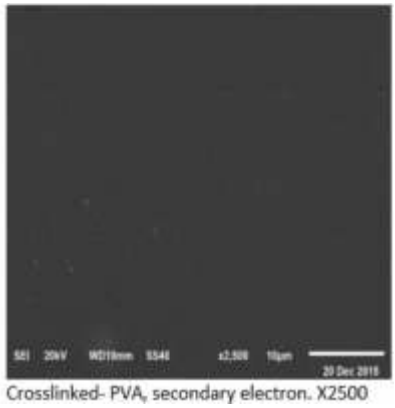

Crosslinked- PVA, secondary electron. X2500

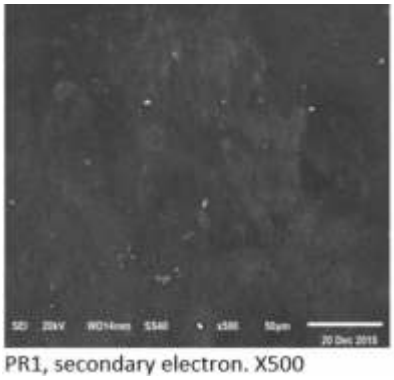

PR1, secondary electron. X500

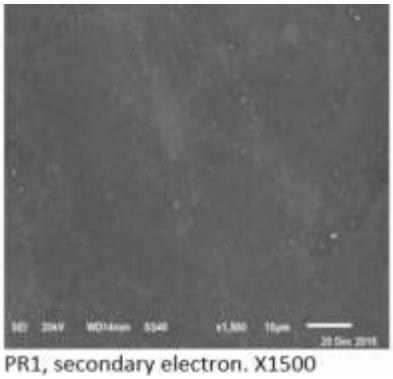

PR1, secondary electron. X1500

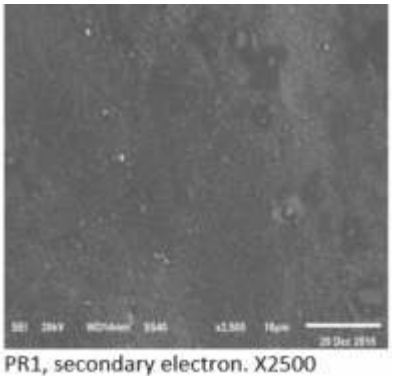

PR1, secondary electron. X2500

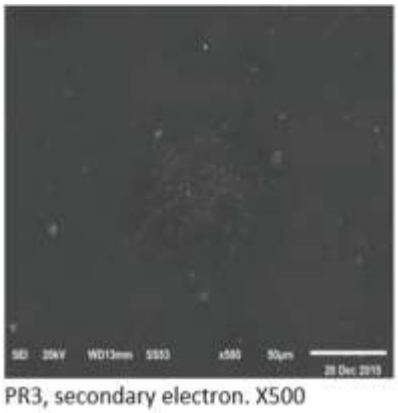

PR3, secondary electron. X500

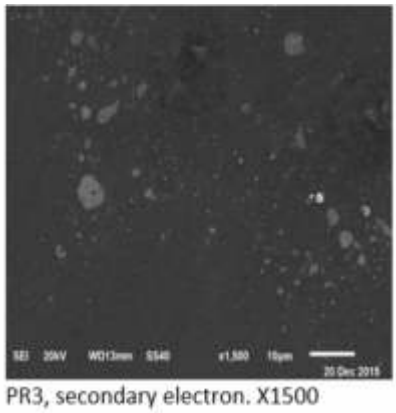

PR3, secondary electron. X1500

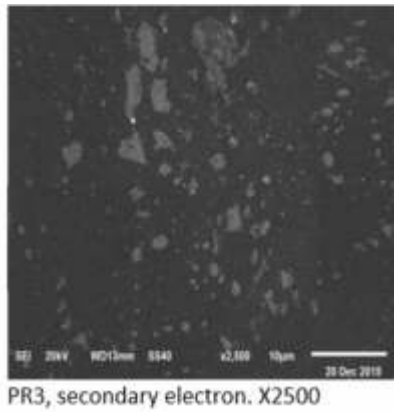

PR3, secondary electron. X2500

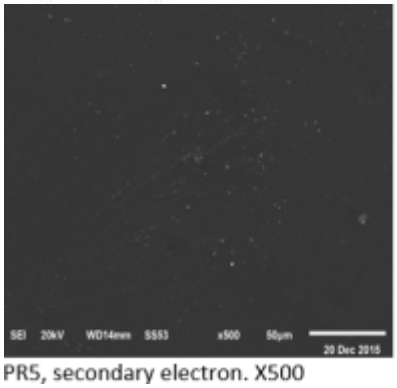

PR5, secondary electron. X500

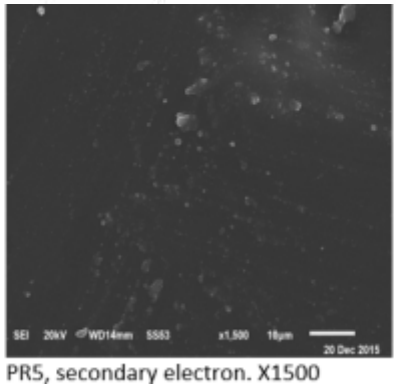

PR5, secondary electron. X1500

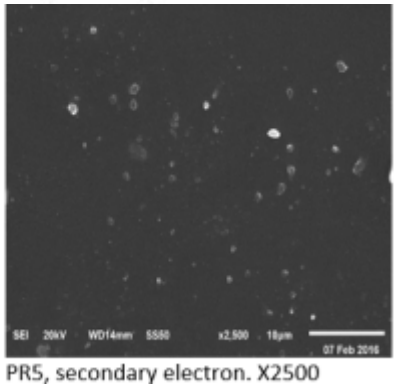

PR5, secondary electron. X2500

After 60 days, the micrographs began to reveal the occurrence of fungal attack, for examples, in nanocomposite PR3. The large spaces between the components of nanocomposite film make it easy to view work of the fungi (Fig. 4). The most damaged nanocomposite was PR3, which underwent bacterial and fungal colonization was very clear (Fig. 4). This has been confirmed by the measurement of weight loss.

Volume : 6 | Issue : 11 | November 2016 | ISSN - 2249-555X | IF : 3.919 | IC Value : 74.50

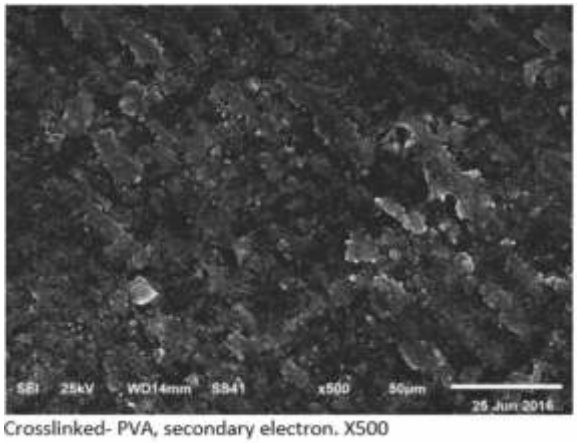

Crosslinked- PVA, secondary electron. X500

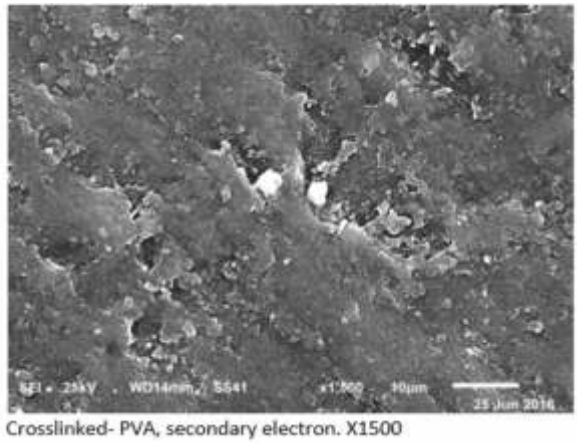

Crosslinked- PVA, secondary electron. X1500

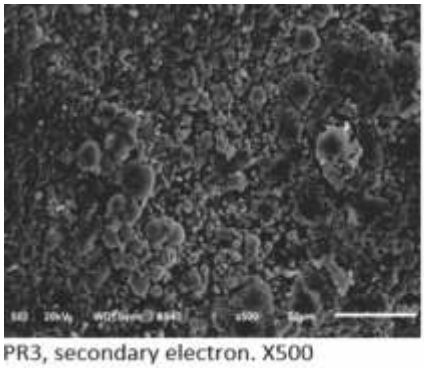

PR3, secondary electron. X500

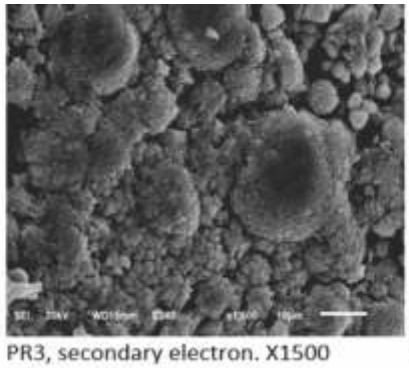

PR3, secondary electron. X1500

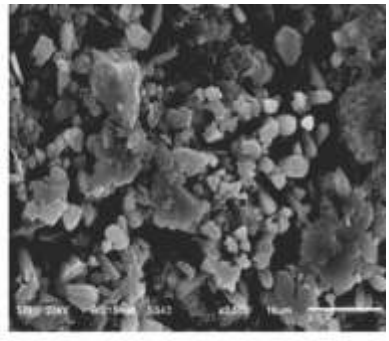

PR3, secondary electron. X2500

Fig. 4. *The SEM micrograph of the surface of crosslinked- PVA and PVA/NRS nanocomposite films (PR1, PR3 and PR5) at magnification x500, 1500 and 2500.*

4.5. Effect of NRS concentration on the thermal history using differential scanning calorimetry (DSC)

DSC is the technique used to determine the quantity of heat either absorbed or released when substances undergo physical or chemical changes It is also noted that the enthalpy

associated with endotherm melting transition decreased with increasing NRS content while the peak position, The tendency of an apparent disproportional reduction in enthalpy with a increase of NRS content implies a rapid decrease of the degree of crystallinity of PVA due to mixing with NRS[30]. The intensity and enthalpy associated with exothermic crystalline peak decreased with increasing NRS content in the PVA/NRS nanocomposite films, while its position is slightly influenced. In addition, the glass transition temperature disappears with increasing concentration of NRS in the PVA/NRS nanocomposite films. Besides, the position of the glass transition temperature Tg is shifted towards higher temperatures as the content of NRS increases (PR5-nanocomposite) (table 2) (fig. 5).

Table 2. *The glass phase transition (Tg), melting phase transition (Tm), crystallinity phase transition (Tc) and associated enthalpies (ΔH) of PVA/NRS PVA/NRS nanocomposite films.*

nanocomposite films	Glass phase transition (Tg)		Melting phase transition (Tm)		Crystallinity phase transition (TC)	
	Tg (°C)	*ΔH (J/g)*	*Tm (°C)*	*ΔH (J/g)*	*TC (°C)*	*H (J/g)*
PVA	٧0.٩٢	7.806	193[31]	24.88	152.38	30.42
Crosslinked- PVA	73.22	6.240	173.57	13.98	122.30	16.21
PR1	-	-	168.68	10.38	111.12	11.75
PR2	-	-	167.95	13.79	117.86	14.77
PR3	-	-	166.40	14.25	114.60	14.55
PR4	-	-	161.23	10.90	108.99	11.63
PR5	84.16	6.704	-	-	79.20	0.5294

Volume : 6 | Issue : 11 | November 2016 | ISSN - 2249-555X | IF : 3.919 | IC Value : 74.50

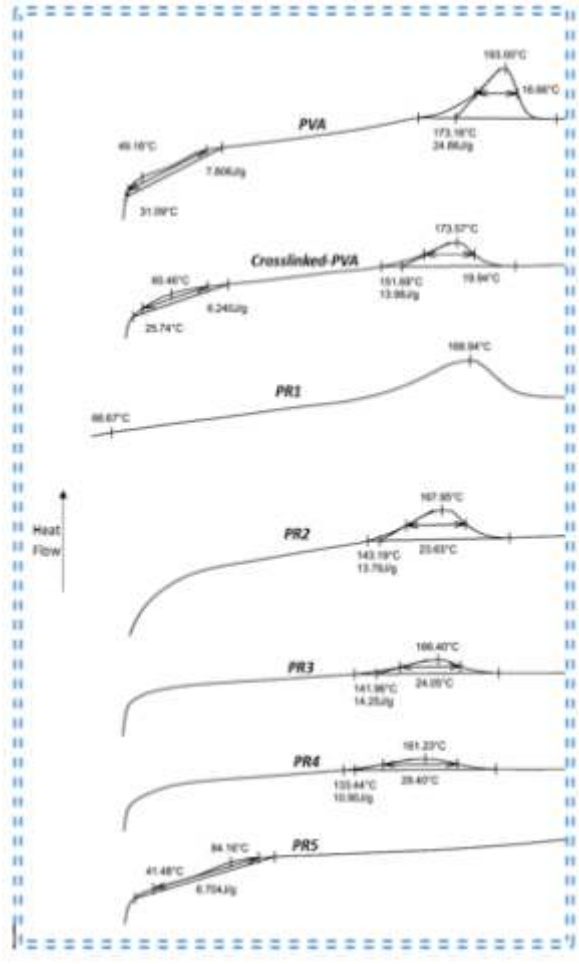

Fig. 5. The Differential scanning calorimetry of PVA, crosslinked- PVA and PVA/NRS nanocomposite films (PR1- PR5) scale to 250 °C.

4.6. Effect of NRS concentrations on the mechanical properties of nanocomposites

4.6.1 Non-irradiated samples

The tensile strength and percent elongation at break for the neat PVA, crosslinked- PVA and PVA/NRS nanocomposite with different concentrations of nano-filler is shown in (Fig. 6). One can notice that the mechanical properties of PVA samples either crosslinked or filled with rice straw decreases with increasing irradiation dose .The tensile strength of neat PVA attains 46.7 MPa and percent of elongation 45 % while for crosslinked- PVA the tensile strength attains 94.23 MPa and percent elongation decrease to18.873% as shown in (Fig. 6). The tensile strength was found to increase with the increase of NRS in PVA to a certain value and then it begins to decrease, as shown in (Fig. 6). The tensile strength of PR1 (1% NRS) attains 76.3 MPa followed by 129 MPa for PR2 (3% NRS). The tensile strength start to decline in the PR3-nanocomposite (5% NRS) due to the relatively poor adhesion between nano-fibers and matrix[32] as at higher concentration there is no perfect wetting due to fiber agglomeration. Elongation at break percent also decreases with increase loading percentage of NRS in PVA matrix and it is minimum for PR5-nanocomposite (10% NRS). Further increase in NRS content leads to a decrease in the tensile strength value. This indicates that the optimum concentration of rice straw in the composites should not exceed 3 % by weight.

4.6.2. Effect of UV irradiation on the prepared composites.

The elongation at break of the nanocomposite decreases with increasing irradiation period, implying a decrease in ductility upon NRS loading. (Fig. 6).

The irradiated PVA/NRS nanocomposite at 50 and 100 hours demonstrated a brittle mode of deformation with decrease in tensile strength compared to non-irradiated PVA/NRS nanocomposite which may be attributed to the change in the morphological structure of the resulted nanocomposite (Techniques 1979; Zhang et al. 2011). Two processes may occur under the effect of unirradiation, firstly at low irradiation doses crosslinking may occur causing increase in tensile strength and decrease in elongation at break. At higher irradiation doses, photo-degradation predominates and higher degree of crosslinking lead to get brittle samples with very low not measurable strain during tensile testing. The presence of rice straw containing carbonyl groups facilitate photo-degradation process of PVA composites.

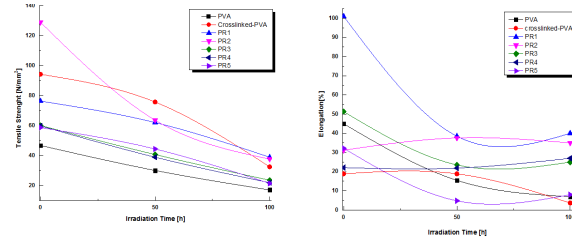

Fig. 6. Tensile strength and Elongation as a function of NRS content at 0, 50 and 100 h UV-irradiation for PVA, crosslinked-PVA and PVA/NRS nanocomposite films.

4.7. Influence of time on water absorption and swelling of nanocomposite films

The swelling degree presented in. (Fig 7 .a-d) show the swelling profiles of the PVA/NRS nanocomposite films as function of time. These figures show that the degree swelling increases with increasing time, reaching the equilibrium degree swelling after ~200 min in most of the PVA/NRS nanocomposite films before and after irradiation. Also, it can be seen that the values of the swelling degree increase with the increase of NRS content in the PVA/NRS nanocomposite films (P duraru et al. 2012; Contents et al. 2009).

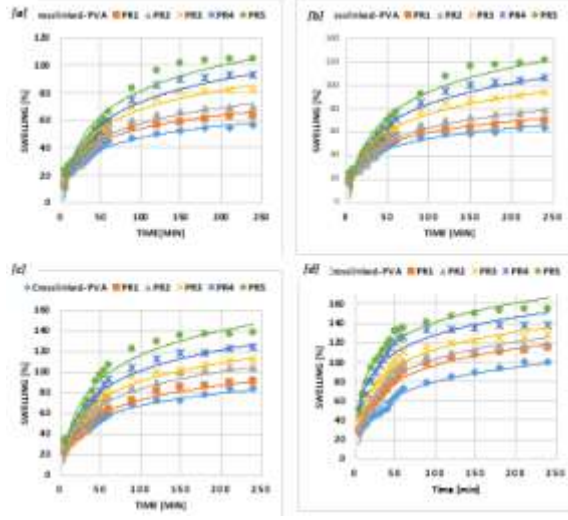

Fig.7. effect of time at (0 h) [a], time at (50 h) [b], time at (100 h) [c] and time at (200 h) [d] on swelling capacity of crosslinked-PVA and PVA/NRS nanocomposite films

Volume : 6 | Issue : 11 | November 2016 | ISSN - 2249-555X | IF : 3.919 | IC Value : 74.50

4.8. Effect of UV-irradiation on Weight loss of the nanocomposite films

The evaluation of degradability under the effect of UV-irradiation is mostly based on the weight loss of materials referring to the erosion of molecules from the solid phase. The UV-irradiation test provides direct indications of degradation. The results show the weight loss of the PVA/NRS nanocomposite films after exposure to UV-irradiation in an accelerated weathering test cycle chamber. All the samples exhibited a quick weight loss in the first 50 hours of exposure of irradiation, and the weight loss slowed down in the subsequent of irradiation period. PVA/NRS nanocomposite films showed a higher weight loss than neat PVA, suggesting their faster degradability. This is because rice straw is more easily degradable than PVA. In fact, the experiment also shows that PR5 sample (10% load) is more likely to degrade, probably due to the reason that of increasing the proportion of rice straw, which benefits the attack for irradiation (fig. 8).

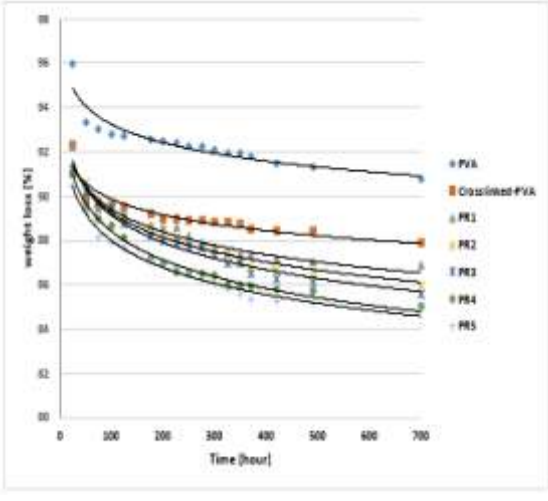

Fig. 8. Weight loss of hot-pressed PVA, PVA crosslinked- and nanocomposite after 700 h of weathering test.

4.9. Effect of soil on Weight loss of PVA/NRS nanocomposite films

The evaluation of biodegradability is mostly based on the weight loss of materials referring to the erosion of molecules from the solid phase. The soil burial test provides indirect indications of biodegradation. Compared with UV - irradiation test, The soil burial method is more effective if the samples are buried in suitable climatic conditions and various populations of microorganisms that are involved[34]. All the samples exhibited a quick weight loss in the first 15 days of soil burial, and the weight loss. Increases in the subsequent burial period. PVA/NRS nanocomposite films showed a higher weight loss than neat PVA, suggesting their faster biodegradability. This is because rice straw is more easily biodegradable than PVA. In fact, it was very difficult to separate rice straw from soil after the first 15 days of burial test attributed to their severe biodegradation under the experiment conditions. The experiment also shows that PR5 sample (10% load) is more likely to biodegrade faster than the other samples, probably due to increase of the proportion of rice straw, which benefits the attack of microorganisms in the soil[35](Fig. 10).

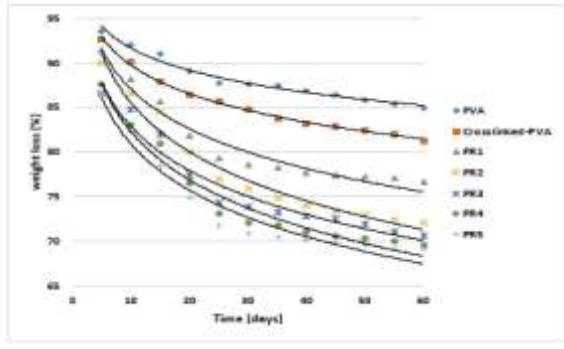

Fig. 9. Weight loss of hot-pressed PVA, PVA crosslinked- and nanocomposite after 60 days of soil burial test.

5. Conclusion

The goal of this study is to investigate the effect of modified nano-rice straw (NRS) on the mechanical, thermal and biodegradable properties of modified nano-rice straw/polyvinyl alcohol nanocomposite films (PVA/NRS nanocomposite films) FT-IR spectroscopy showed that the interaction between PVA and NRS is chemical and physical interaction.

- The XRD results showed that the intensity of the peaks characteristic for the crystallinity of the composites decreases with the increase of NRS content from 1 to 10 wt. % (PR1 to PR5) in comparison with PVA peaks.
- PVA/NRS nanocomposite films of NRS/PVA showed good mechanical properties Also PVA/NRS nanocomposite films during exposure to radiation for 50 and 100 hours got her continuous decrease in the tensile strength till 200h exposure and 60 days of burial test.
- SEM micrograph indicated good dispersion of NRS into the matrix and the micrographs to reveals the occurrence of fungal attack (PR3) after 60 days.
- The swelling of the PVA/NRS nanocomposite films showed that it increases with increase percentage of nano-rice straw.

6. Reference

[1] L. Tighzert, I. Vroman, "Biodegradable Polymers," vol. 2, pp. 307344, 2009.[2]I. [1] L. Tighzert, I. Vroman, "Biodegradable Polymers," vol. 2, pp. 307–344, 2009.
[2] I. Sakurada, Polyvinyl Alcohol Fibers, vol. 20. CRC Press, 1985.
[3] F. Mano, I. M. Aroso, S. Barreiros, J. P. Borges, R. L. Reis, A. R. C. Duarte, and A. Paiva, "Production of Poly(vinyl alcohol) (PVA) Fibers with Encapsulated Natural Deep Eutectic Solvent (NADES) Using Electrospinning," ACS Sustain. Chem. Eng., p. 150924160611006, 2015.
[4] P. G. Allison, R. D. Moser, M. Q. Chandler, O. G. Rivera, J. R. Goodwin, E. R. Gore, and C. A. W. Jr, "Mechanical , Thermal , and Microstructural Analysis of Polyvinyl Alcohol / Montmorillonite Nanocomposites," vol. 2015, 2015.
[5] K. Leja and G. Lewandowicz, "Polymer biodegradation and biodegradable polymers - A review," Polish J. Environ. Stud., vol. 19, no. 2, pp. 255–266, 2010.
[6] E. A. Kamoun, X. Chen, M. S. Mohy, and E. S. Kenawy, "Crosslinked poly (vinyl alcohol) hydrogels for wound dressing applications : A review of remarkably blended polymers," Arab. J. Chem., vol. 8, no. 1, pp. 1–14, 2015.
[7] R. Purwar, S. Sharma, P. Sahoo, and C. M. Srivastava, "Flexible sericin/polyvinyl alcohol/clay blend films," Fibers Polym., vol. 16, no. 4, pp. 761–768, 2015.
[8] K. Qiu and A. N. Netravali, "Fabrication and characterization of biodegradable composites based on microfibrillated cellulose and polyvinyl alcohol," Compos. Sci. Technol., vol. 72, no. 13, pp. 1588–1594, 2012.
[9] Y. Wu, S. Wang, D. Zhou, Y. Zhang, X. Wang, and R. Yang, "Biodegradable polyvinyl alcohol nanocomposites made from rice straw fibrils: Mechanical and thermal properties," J. Compos. Mater., 2012.
[10] G. I. Lawal, S. A. Balogun, and E. I. Akpan, "Review of Green Polymer Nanocomposites," vol. 11, no. 4, pp. 385–416, 2012.
[11] Q. Cheng, S. Wang, and T. G. Rials, "Poly(vinyl alcohol) nanocomposites reinforced with cellulose fibrils isolated by high intensity ultrasonication," Compos. Part A Appl. Sci. Manuf., vol. 40, no. 2, pp. 218–224, 2009.

Volume : 6 | Issue : 11 | November 2016 | ISSN - 2249-555X | IF : 3.919 | IC Value : 74.50

[12] W. Zhang, X. Yang, C. Li, M. Liang, C. Lu, and Y. Deng, "Mechanochemical activation of cellulose and its thermoplastic polyvinyl alcohol ecocomposites with enhanced physicochemical properties," Carbohydr. Polym., vol. 83, no. 1, pp. 257–263, 2011.
[13] R. Bana and a. K. Banthia, "Mechanical and Thermal Analysis of Poly (Vinyl-Alcohol) and Modified Wood Dust Composites," J. Wood Chem. Technol., vol. 31, pp. 218–232, 2011.
[14] O. M. P duraru, D. Ciolacu, R. N. Darie, and C. Vasile, "Synthesis and characterization of polyvinyl alcohol/cellulose cryogels and their testing as carriers for a bioactive component," Mater. Sci. Eng. C, vol. 32, no. 8, pp. 2508–2515, 2012.
[15] P. D. Evans, N. L. Owen, S. Schmid, and R. D. Webster, "Weathering and photostability of benzoylated wood," Polym. Degrad. Stab., vol. 76, no. 2, pp. 291–303, 2002.
[16] A. Temiz, U. C. Yildiz, I. Aydin, M. Eikenes, G. Alfredsen, and G. Çolakoglu, "Surface roughness and color characteristics of wood treated with preservatives after accelerated weathering test," Appl. Surf. Sci., vol. 250, no. 1–4, pp. 35–42, 2005.
[17] R. Bana and a. K. Banthia, "Green Composites: Development of Poly(Vinyl Alcohol)-Wood Dust Composites," Polym. Plast. Technol. Eng., vol. 46, no. June 2013, pp. 821–829, 2007.
[18] J. Gaume, P. Wong-Wah-Chung, A. Rivaton, S. Thérias, and J.-L. Gardette, "Photochemical behavior of PVA as an oxygen-barrier polymer for solar cell encapsulation," RSC Adv., vol. 1, no. 8, p. 1471, 2011.
[19] J. L. Ferreira, M. J. Melo, and A. M. Ramos, "Poly(vinyl acetate) paints in works of art: A photochemical approach. Part 1," Polym. Degrad. Stab., vol. 95, no. 4, pp. 453–461, 2010.
[20] S. Wei, V. Pintus, and M. Schreiner, "Photochemical degradation study of polyvinyl acetate paints used in artworks by Py-GC/MS," J. Anal. Appl. Pyrolysis, vol. 97, pp. 158–163, 2012.
[21] S. S. M. Pawde, K. Deshmukh and Parab, "Preparation and Characterization of Poly(vinyl alcohol) and Gelatin Blend Films," Polym. Polym. Compos., vol. 109, pp. 1328–1337, 2008.
[22] R. Silverstein, F. Webster, and D. Kiemle, "Spectrometric Identification of Organic Compunds." p. 550, 2005.
[23] X. Colom, F. Carrillo, F. Nogués, and P. Garriga, "Structural analysis of photodegraded wood by means of FTIR spectroscopy," Polym. Degrad. Stab., vol. 80, no. 3, pp. 543–549, 2003.
[24] K. Ma, F. R. Voort, J. Sedman, and a. a. Ismail, "Stoichiometric determination of hydroperoxides in fats and oils by fourier transform infrared spectroscopy," J. Am. Oil Chem. Soc., vol. 74, no. 8, pp. 897–906, 1997.
[25] P. Calvini and a. Gorassini, "FTIR – Deconvolution Spectra of Paper Documents," Restaurator, vol. 23, no. 1, pp. 48–66, 2002.
[26] Y. C. Ching, A. Rahman, K. Y. Ching, N. L. Sukiman, and C. H. Chuah, "Preparation and Characterization of Polyvinyl Alcohol- Based Composite Reinforced with Nanocellulose and Nanosilica," vol. 10, no. 2, pp. 3364–3377, 2015.
[27] Y. Liu, M. Huang, D. Cai, J. Sun, C. Qin, L. Dai, and J. Wang, "Effect of nano-SiO2 on the compatibility of PVA/RSF blend," Iran. Polym. J., vol. 21, no. 8, pp. 523–530, 2012.
[28] W. Zhang, X. He, C. Li, X. Zhang, C. Lu, X. Zhang, and Y. Deng, "High performance poly (vinyl alcohol)/cellulose nanocrystals nanocomposites manufactured by injection molding," Cellulose, vol. 21, no. 1, pp. 485–494, 2014.
[29] S. K. Ozaki, M. B. B. Monteiro, H. Yano, Y. Imamura, and M. F. Souza, "Biodegradable composites from waste wood and poly(vinyl alcohol)," Polym. Degrad. Stab., vol. 87, pp. 293–299, 2005.
[30] A. Abdulkhani, E. Hojati Marvast, A. Ashori, Y. Hamzeh, and A. N. Karimi, "Preparation of cellulose/polyvinyl alcohol biocomposite films using 1-n-butyl-3-methylimidazolium chloride," Int. J. Biol. Macromol., vol. 62, pp. 379–386, 2013.
[31] S. Contents, P. Class, and J. E. Mark, "Polymer data handbook," 2009.
[32] G. C. Li, J. Chen, Q. Li, and T. Yang, "Biodegradable Composites from Pinewood Sawdust and Polyvinyl Alcohol Adhesives," Adv. Mater. Res., vol. 281, no. 1788, pp. 59–63, 2011.
[33] V. S. Techniques, "Induction and Measurement of Glassy-State Relaxations by Vapor Sorption Techniques," vol. 17, pp. 1757–1770, 1979.
[34] E. Chiellini, P. Cinelli, F. Chiellini, and S. H. Imam, "Environmentally degradable bio-based polymeric blends and composites," Macromol. Biosci., vol. 4, no. 3, pp. 218–231, 2004.
[35] L. Yu, Biodegradable polymer blends and composites from renewable resources. 2009.